



저작자표시-비영리-변경금지 2.0 대한민국

이용자는 아래의 조건을 따르는 경우에 한하여 자유롭게

- 이 저작물을 복제, 배포, 전송, 전시, 공연 및 방송할 수 있습니다.

다음과 같은 조건을 따라야 합니다:



저작자표시. 귀하는 원저작자를 표시하여야 합니다.



비영리. 귀하는 이 저작물을 영리 목적으로 이용할 수 없습니다.



변경금지. 귀하는 이 저작물을 개작, 변형 또는 가공할 수 없습니다.

- 귀하는, 이 저작물의 재이용이나 배포의 경우, 이 저작물에 적용된 이용허락조건을 명확하게 나타내어야 합니다.
- 저작권자로부터 별도의 허가를 받으면 이러한 조건들은 적용되지 않습니다.

저작권법에 따른 이용자의 권리는 위의 내용에 의하여 영향을 받지 않습니다.

이것은 [이용허락규약\(Legal Code\)](#)을 이해하기 쉽게 요약한 것입니다.

[Disclaimer](#)

Thesis for the Degree of Master of Engineering

Assessing the feasibility of UAV
photogrammetry for sequential coastal
monitoring



by

Seong Heon Kim

Department of Spatial Information Engineering

The Graduate School

Pukyong National University

February 2020

Assessing the feasibility of UAV
photogrammetry for sequential coastal
monitoring

(시계열 연안 모니터링을 위한 사진측량
UAV 시스템의 적용 가능성 평가)

Advisor : Prof. Jin Soo Kim



by
Seong Heon Kim

A thesis submitted in partial fulfillment of the requirements
for the degree of
Master of Engineering
in Department of Spatial Information Engineering, The Graduate School,
Pukyong National University

February 2020

Assessing the feasibility of UAV photogrammetry for
sequential coastal monitoring

A dissertation
by
Seong Heon Kim

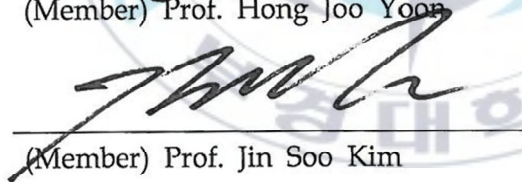
Approved by:



(Chairman) Prof. Chul Uong Choi



(Member) Prof. Hong Joo Yoon



(Member) Prof. Jin Soo Kim

February 2020

CONTENTS

Contents	I
List of figures	III
List of Tables	V
List of acronyms	VI
1. Introduction	1
1.1. Background	1
1.2. Previous study	4
1.3. Objective	9
2. Methodology	12
2.1. Study area	12
2.2. Data collection	13
2.2.1. UAV photogrammetry	13
2.2.2. GNSS surveying	16
2.2.3. TLS laser scanning	19
3. Results and Discussion	22
3.1. Accuracy assessment	22
3.2. Quality estimation	25
3.3. Beach vertical change detection	30
3.4. Shoreline detection with image segmentation	33
3.5. Shoreline change analysis	36
4. Conclusions	39
References	41

LIST OF FIGURES

Fig. 1. Workflow in this study.	11
Fig. 2. The study area. (a) test field for this study is Imlang Beach in Busan, Korea, (b) aerial photographic in Imlang beach, (c) panoramic photographic in Imlang beach.	13
Fig. 3. UAV photogrammetry. UAV path on 25 February (a) and (b) UAV path on 20 May, UAV orthomosaic on 25 February (c), UAV orthomosaic on 20 May (d).	16
Fig. 4. Network-RTK surveying in study area. (a) Location of Network-RTK field campaign, (b) Network-RTK surveying on benchmark and (c) Network-RTK surveying on artificial feature.	18
Fig. 5. Location of calibration data.	18
Fig. 6. TLS surveying in study area. (a) TLS surveying on the road and (b) TLS surveying on the beach, (c) station view, (d) acquired point clouds.	20
Fig. 7. Marking the location of the data to be used in the study. (a) Beach area and cross-shore and (b) DEM derived from UAV photogrammetry and TLS surveying.	27
Fig. 8. Graph of cross-shore profiles between UAV photogrammetry in February (red) and TLS surveying (black).	29
Fig. 9. Graph of cross-shore profiles between UAV photogrammetry in February (red) and UAV photogrammetry in May (green).	31
Fig. 10. Before and after beach construction in the study area. (a) before	

beach road construction, (b) after beach road construction and (c) before sidewalk road construction, (d) after beach sidewalk road construction.

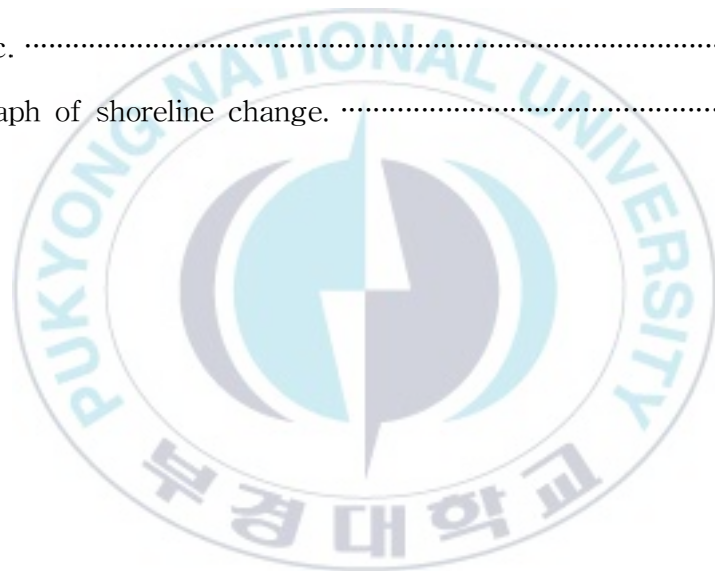
..... 33

Fig. 11. Image segmentation. (a) Multiresolution segmentation on 25 February, (b) multiresolution segmentation on 20 May and (c) spectral difference segmentation on 25 February, (d) spectral difference segmentation on 20 May. 35

Fig. 12. The acquired shoreline in February and May. 36

Fig. 13. Indicate that baseline, shorelines, and transect in aerial photographic. 37

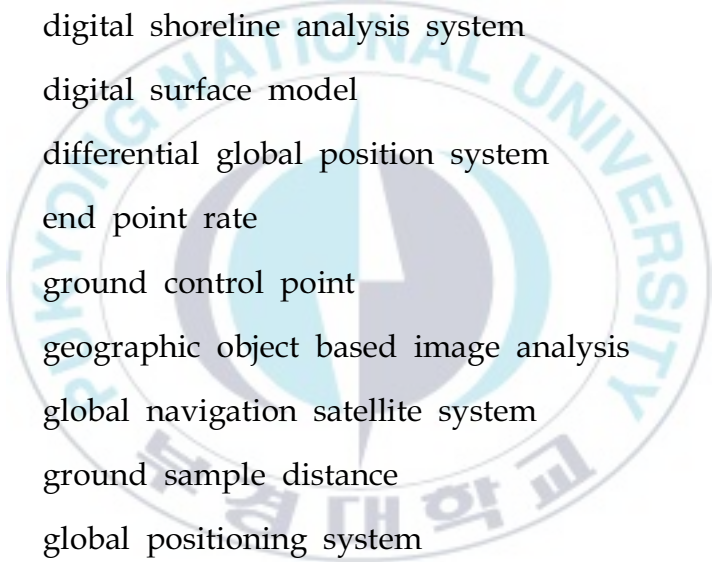
Fig. 14. Graph of shoreline change. 38



LIST OF TABLES

Table 1. Orientation error for each TLS station (unit : m)	21
Table 2. RMSE statistics by 25 ground control points (unit: m)	25
Table 3. RMSE statistics by 13 check points (unit: m)	25
Table 4. Comparison of volumes between TLS DEM and UAV DEM in February	28
Table 5. Difference of vertical between TLS DEM and UAV DEM in February (Unit: m)	30
Table 6. Difference of vertical between UAV DEM in February and May (Unit: m)	32
Table 7. Comparison of volumes between UAV DEM in February and May	32

LIST OF ACRONYMS



CP	check point
CS	cross shore
DEM	digital elevation model
DGPS	differential global position system
DSAS	digital shoreline analysis system
DSM	digital surface model
DGPS	differential global position system
EPR	end point rate
GCP	ground control point
GEOBIA	geographic object based image analysis
GNSS	global navigation satellite system
GSD	ground sample distance
GPS	global positioning system
IDW	inverse distance weighted interpolation
IMU	inertial measurement unit
IPCC	UN intergovernmental panel on climate change
KHOA	korea hydrographic and oceanographic agency
LiDAR	light detection and ranging
NSM	net shoreline movement
MOF	ministry of oceans and fisheries
RMS	root mean square

RMSE	root mean square error
SfM	structure from motion
TIN	triangulated irregular network
TLS	terrestrial laser scanning
UAV	unmanned aerial vehicle



김 성 현

부 경 대 학 교 대 학 원 공 간 정 보 시 스템 공 학 과

요 약

본 연구는 UAV photogrammetry를 이용하여 수직 프로파일 및 체적 분석으로 연안 지역을 모니터링하고, 해안선의 변화 탐지 가능성을 평가하는 것에 목적을 둔다. 부산광역시 기장군 임랑 해수욕장을 연구 대상 지역을 선정했고, Inspire 2 UAV에 탑재된 Zenmuse X7 camera를 이용하여 2019년 2월과 5월 총 2차례에 걸쳐 고도 100m에서 UAV photogrammetry를 실시했다. 2월에 수집된 총 사진의 수는 245장이며 ground sample distance (GSD)는 1.59 cm, 5월의 경우 240장이며 GSD는 1.61 cm로 수집했다. UAV photogrammetry를 통한 수직 프로파일과 체적 분석 등 연안 모니터링의 가능성을 평가하기 위해 terrestrial laser scanning (TLS) surveying을 수행했다. 수집된 데이터는 검증자료로 이용했다. UAV photogrammetry에 사용할 ground control point (GCP) 38개와 TLS surveying에 사용할 21 지점에 대하여 network-real time kinematic (Network-RTK)방법을 이용하여 좌표를 수집했다. UAV 데이터를 이용하여 Structure from Motion (SfM) algorithm을 통해 영상정합 과정을 거쳐, 정사영상 및 point clouds, digital elevation model (DEM)을 제작했다. 또한 수집된 21개 지점의 TLS point clouds는 registration 작업을 수행했다. 25개의 GCPs 기반으로 변형조정 결과, 위치 정확도를 나타내는 GCPs의 root mean square error (RMSE)는 2월의 경우 X, Y, Z 방향으로 각각 0.010 m, 0.008 m, 0.016 m로 나타났고, 5월은 0.012 m, 0.011 m, 0.018 m로 나타났다. 13개 check point로 검증한 결과 RMSE는 2월의 경우 0.015 m, 0.017 m, 0.040 m, 5월은 0.018 m, 0.015 m, 0.035 m로 나타났다. 연안 모니터링의 UAV photogrammetry의 정확도 평가를 위해 UAV, TLS에서 수집된 point clouds를 DEM로 생성했다. 해변에 대한 UAV DEM과 TLS DEM에서 전체 평균 높이 차이는 약 0.017 m, RMSE는 0.032 m로 나타났고, 체적 차이는 0.7%로 나타났다. 따라서 고정밀 TLS와의 비교 결과에 비춰볼 때, UAV photogrammetry는 연안 프로파일 작성에 그 활용성이 충분히 있는 것을 확인할 수 있었다. 반면 2월 UAV DEM과 5월 UAV DEM의 전체 평균 높이 차는 약 0.165 m, 체적 차이는 6.6%로 나타났다. 최종적으로 수집된 UAV 정사영상을 image segmentation을 적용하여 해안선을 추출했으며, 해안선 분석 프로그램인 Digital shoreline analysis system (DSAS) 4.3을 이용하여 해안선 변화를 분석했다. 그 결과 임랑 해수욕장 남서쪽 부분에서 해안선이 후퇴하는 경향이 나타났다. 이상의 연구 결과에 비춰볼 때, 주기적, 시계열적 연안침식 프로파일 작성과 모니터링을 위해 UAV photogrammetry 기술은 효율성과 정확도 측면에서 그 활용성이 매우 클 것으로 기대된다.

1. Introduction

1.1. Background

The coastal area, which borders the sea and land, is highly useful as a place where mankind has been active for a long time due to conditions such as flat areas, fertile soil such as the delta, and other areas and exchanges. Coastal areas in the world live adjacent to the sea is live about 300 million people (Martínez et al., 2007; Ministry of Oceans and Fisheries, 2017; Woodroffe, 2002). Recently, coastal areas have been exposed around the world from disasters. Global warming caused by climate change like strong typhoons and rising sea levels has been affected for the disaster, and coastal areas has been seriously damaged (Defeo et al., 2009; Gonçalves and Henriques, 2015; Kim et al., 2013). According to the UN Intergovernmental Panel on Climate Change (IPCC) fifth report released in September 2013, sea level rise will rise 0.45 to 0.85 m in the future. In the fourth report released in February 2007, the maximum value of sea level rise is 0.59 m. The difference in the maximum values of the fourth and fifth reports is 0.23 m. According to the Korea Hydrographic and Oceanographic Agency (KHOA) tide station data from the national average, the average rate is rising sea levels that the West Sea 1.06 mm/yr, and the South Sea, 2.26 mm/yr, the East Sea 3.35 mm/yr, the Jeju-do, 4.56 mm/yr. In particular, Pohang-si on the East Sea indicated 5.98 mm/yr. The East Sea was 2.0 mm/yr higher than the global average. This is a serious problem for coastal safety in Korea. This means that sea level rise is

already an important issue (Ministry of Oceans and Fisheries, 2017). Sea level rise causes coastal erosion, affect enormous damage to living people in coast. As a result, coastal management is essential.

Coastal monitoring has been considered for efficient coastal management to prevent coastal erosion, it is refers to the activities necessary to protect. Coastal monitoring continuously observes the current state of the coast and shoreline. It is necessary to protect and maintain important coasts through coastal monitoring, such as predicting the appearance of coasts due to future state changes (Douglas and Crowell, 2012; Kim et al., 2013). Coastal monitoring was assessed for shoreline changes, beach volume changes, etc by using a variety of methods. There is remote video monitoring in the case of ground based coastal monitoring. It can provide spatial and time-series information about coast changes, such as retreat of shoreline etc by placing a number of video cameras on the coast. Argus Station developed by the Coastal Imaging Lab of Oregon State University. It was used to survey shoreline changes and define shoreline (Holman and Stanley, 2007; Kim et al., 2013). Other ground based equipment is the Global Navigation Satellite System (GNSS). It is a sophisticated technology that can collect high quality data in terms of spatial and temporal resolution. The received data from satellites can be acquire 3-dimensional coordinate. GNSS was used for coastal monitoring activities such as measuring height changes on the beach (Morton et al., 1993; Suanez et al., 2010).

There is a remote sensing method using aircraft and satellites, as a coastal monitoring method based on aviation. Aerial photographic surveying were known as the only source of coastal map from 1927 to 1980 (Alesheikh, 2007). Remote sensing has the advantage of acquiring

high-resolution image in wide spatial, periodic scale with the recent development of aircraft and satellites. Development in the technology of sensors attached to satellites, have enabled the acquisition of images with higher spatial-resolution of 20–50 cm (Papakonstantinou et al., 2016; Tuner et al., 2012). Some researchers have conducted coastal monitoring studies on coastal erosion and shoreline transformation using various satellites, such as WorldView-2, SPOT and Landsat (Li and Daman, 2010; Maglione et al., 2014; Nayak, 2002; Seker et al., 2008). There is airborne light detection and ranging (LiDAR), which consists of a global positioning system (GPS) and a laser scanner. This equipment can generate 3-dimensional point clouds at intervals of about 10 points/m by directly firing laser pulses to survey the return time of the reflected laser pulse through a combination with the location and direction. Airborne LiDAR can be survey to wide, because it operates on an airplane platform. Airborne LiDAR technology can improve the accuracy of mapping coastal areas. It can produce digital surface model (DSM) and digital elevation model (DEM) for terrain analysis through the acquired point clouds in coastal area (Jansen, 2018).

Coastal monitoring has been performed using traditional surveying techniques, such as video monitoring, GNSS, remote sensing, and airborne LiDAR. Traditional surveying techniques on coastal monitoring have high time-consuming, expensive, labor-intensive when acquiring data over large areas (Yoo and Oh, 2016). Airborne LiDAR, remote sensing are affected by weather, spatial-resolution, periodic characteristics, and operating costs are high. In addition, the access of the general public is limited. It remains a limited technology, because of its high cost (Laidlaw, 2017). Satellites have greatly improved the spatial resolution of satellite images over the years, but it is difficult to

detect rapid coastal changes such as shoreline changes, coastal profiles, coastal mapping, due to periodic disadvantage (Casella et al., 2016; Topouzelis et al., 2017)

Coastal area consists of complex topographical features, it is rapidly changing due to wind, waves, and tidal waves. Frequent coastal monitoring are required to detect and quantify coastal change to efficiently manage the coastal (Gonçalves and Henriques, 2015; Jeong et al., 2018; Topouzelis et al., 2017). Coastal monitoring using new methods are needed, because of disadvantage with traditional surveying techniques. An alternative is UAV photogrammetry which use Unmanned Aerial Vehicles (UAV) and high-performance camera.

1.2. Previous study

UAV photogrammetry can acquire high-resolution orthomosaic at low cost compared with traditional surveying techniques (Goncalves and Henriques, 2015; Uysal et al., 2015). It can collect and analyze data quickly, although the measurement range is smaller than remote sensing. UAV photogrammetry can be used to collect data at any time, which is advantageous for studies requiring periodic monitoring (Casella et al., 2014; Jiménez López and Mulero-Pázmány, 2019).

UAV photogrammetry was used in periodic terrain monitoring studies, it has been since the structure from motion (SfM) algorithm was applied to the UAV photogrammetry. The SfM algorithm is a method that can be collected with 3-dimensional point clouds data that can detail the terrain, such as Airborn LiDAR based on collected photographic images. It is also possible to estimate the camera position

and orientation from numerous 2D images taken at various points, and restoring the collected image to a three-dimensional structure. This algorithm matches the extracted keypoints from the two images and then identifies the epipolar geometry using the corresponding keypoints. It allows the relative movement of the two cameras and the method of restoring the 3-dimensional structure of the object scene (Lee et al., 2015). The point clouds are generated from relative coordinate, as the point clouds derived using SfM algorithm in the collected UAV images, lack scale and orientation. Relative coordinates need to be converted to real coordinates. This can be converted to real coordinates using a ground control point (GCP) with real coordinates. GCP can be collected by GNSS and calculated by real coordinates. As a result, 3-dimensional point clouds can be reproduced with the same actual size (Westoby et al., 2012), and the SfM algorithm can be used to reconstruct terrain such as point clouds collected by LiDAR from the UAV photogrammetry orthomosaic (Long et al., 2016; King et al., 2017).

Nex and Remondino (2014) reported that UAV photogrammetry is a fast and affordable way to obtain information in areas such as agriculture, forestry, archeology, architecture, environment, and transportation. Lomax et al. (2005) reported that in ocean surveys, UAV photogrammetry can be used to detect temperature, bathymetry, ice distribution, sea color detection, and surface waves.

A research related to coastal monitoring is being carried out, based on such advantages as periodic aspects, and low cost in the UAV photogrammetry. In case of domestic studies, Kim et al. (2015) conducted beach surveying and wave-induced current surveying using fixed wing and rotary wing UAV. It was conducted a beach surveying on the Manseong-ri Black sand beach in Yeosu-si using a fixed wing

UAV. As a result, beach surveying using fixed wing UAV photogrammetry was able to estimate sand volume more accurately than conventional methods. A dye was added to the sea to determine the wave-induced current. As a result, UAV photogrammetry using rotary wing UAV was able to identify wave-induced current without being affected by external force such as wind. Lee et al. (2015) conducted on shoreline extraction using rotary wing UAV. A study was conducted during the period of maximum spring range around January 2015. UAV photogrammetry was performed at an hours interval at the Balam-alae beach in Chungcheongnam-do. As a result, the collected orthomosaic through UAV photogrammetry was extracted to the shoreline by time using the sobel filtering operation. It is very difficult to construct accurate shoreline data due to the frequent changing nature of the coastal topography. It reported that reliable shoreline data could be constructed, if the frequent surveying was available by UAV photogrammetry. Lee et al. (2016) were constructed orthomosaic, DSM by UAV photogrammetry, and GCP survey at Buan beach. A total of thirty-three CPs surveys were conducted with a virtual reference station (VRS) survey to evaluate the accuracy of UAV positioning for beach areas. As a result, the horizontal standard error was ± 5.8 cm and ± 4.7 cm in the X, Y direction, respectively. The standard error for elevation was ± 8.6 cm in the Z direction. It is reported that the 3-dimensional topographic modeling using UAV photogrammetry can be used as the topographical results in the beach area.

In the case of international studies, Mancini et al. (2017) used to UAV photogrammetry to perform volume observations of about 600 m long rocky sea cliffs in Sant'Andrea, Italy. UAV photogrammetry was

performed to investigate rocky sea cliffs at altitude 50 m. As a result, UAV photogrammetry proved to be a fast and automated tool for damage analysis of sea cliff slopes. Papakonstantinou et al. (2016) obtained orthomosaic of 3 cm and 5 cm for two beaches by UAV photogrammetry. Two acquired orthomosaic have been extracted shoreline using geographic object based image analysis (GEOBIA). A fuzzy classification was conducted to identify sand, rubble, and rocks in orthomosaic wetland. Drummond et al. (2015) used to fixed-wing UAV photogrammetry to acquire point cloud before and after the typhoon of Narrabeen-Collaroy Beach in Australia, and evaluated the volume change. It is represented a difference of about 1% between before and after the typhoon, which it proved that UAV photogrammetry provide offshore researchers with tools for mapping, measuring and coastal monitoring. Ventura et al. (2018) constructed a habitat map for seafloor around the coast using the acquired orthomosaic by UAV photogrammetry. The seafloor habitat map was classed to rocky coast, seagrace, and sandy areas using object-based image analysis technique. It is reported that the possibility of UAV photogrammetry establishing coast seafloor habitat map. UAV photogrammetry suggest various detection possibilities for coastal.

Many studies have been conducted to evaluate the accuracy of point clouds and DSMs by using UAV photogrammetry in coast. UAV photogrammetry can generate point clouds that can describe the terrain in detail by processing acquired images with SfM algorithm in coast area. But areas characterized by flat surfaces (sand, water) of the coast in UAV images are difficult to extract matching shapes (points) from the coast surface. The obtained UAV point clouds by applying the SfM algorithm are difficult to represent the beach (Mancini et al., 2013). As

a result, several researchers evaluated the accuracy of the differences by comparing the produced results based on various traditional surveying techniques with reference data to verify the collected data through the SfM algorithm in UAV photogrammetry.

Long et al. (2016) used UAV photogrammetry to survey coastal mud flats at different altitudes and constructed about 2–5 cm of orthomosaic, DSM in June, September, and October. The accuracy of the constructed DSM was evaluated using the GNSS profile. Root mean square error (RMSE) was about 10–17 cm. It is evaluated that UAV photogrammetry can construct accurate data even on coastal tidal flats. Gonçalves and Henriques. (2015) surveyed in the coast using the mounted digital camera on a commercial UAV. The acquired images was produced orthomosaic and DSM using Agisoft Photoscan software and analyzed the accuracy. As a result of accuracy evaluation, the vertical accuracy can achieve an RMSE of less than 5 cm using Differential Global Position System (DGPS) surveying for a produced DSM with a spatial resolution of 10 cm. Mancini et al. (2013) generated 3-dimensional point clouds using acquired images from UAV photogrammetry by applying the SfM algorithm. TLS surveying was conducted for the same area. The acquired point clouds by UAV photogrammetry were verified by comparison with the acquired point clouds by TLS surveying. The result indicated a vertical difference of 0.05 m, root mean square (RMS) is about 0.19 m. The DSM generated at each point cloud was compared with GNSS to analyze vertical absolute accuracy, which was about 0.011 m. Guillet et al. (2018) conducted UAV photogrammetry and LiDAR surveying on Truc Vert sand beaches where erosion occurred in 2012, 2014, and 2017 for a total of three years. The acquired point clouds constructed a DSM with a

spatial resolution of 0.04 m using GIS tool. As a result of cross-shore profile using cross-shore (CS), sand beach surveyed a change in volume with each year of observation. This suggests that quantitative survey of patterns and magnitude of sand beach recovery are possible using UAV photogrammetry.

The applied SfM algorithm in image processing of UAV photogrammetry was not only able to generate point clouds that could represent the terrain, but confirmed the accuracy of the number of cm in the evaluation results of the traditional surveying techniques and accuracy. Therefore, UAV photogrammetry is evaluated in a reliable method for coastal monitoring activities (Drummond et al., 2015; Nex and Remondio., 2014).

1.3. Objective

The coastal erosion survey conducted by national and local governments evaluates coastal erosion monitoring results for beaches distributed nationwide using Network-real time kinematic (RTK) for a certain period of time each year. Network-RTK is conducting only section surveys, there is a lack of quantitative evaluation of the entire beach.

A UAV is equipped with high-ability cameras and sensors to acquire high-resolution orthomosaic in conducting coastal monitoring. It is overcome the limitations of information collection such as spatial resolution, periodic, cost of remote sensing and traditional surveying techniques. UAV photogrammetry is advantage for studies requiring

periodic terrain monitoring. The SfM algorithm was applied to the acquired images, enabling precise 3-dimensional point clouds collection. As a result, it has been applied to many coastal monitoring studies at abroad. There are few coastal monitoring cases using UAV photogrammetry in Korea.

This study aims to comprehensively evaluate coastal monitoring such as area, volume, shoreline changes by using UAV photogrammetry for coast. UAV photogrammetry was conducted at Imlang beach for time-series analysis in February and May 2019. Point clouds, orthomosaic are generated from the acquired images through UAV photogrammetry. Location accuracy verify using the surveyed GCPs by Network-RTK, during the process of bundle adjustment and triangulation method. The absolute accuracy verification conducts from the generated result using the CPs. The acquired DEM through TLS surveying verify to the acquired DEM through UAV photogrammetry as reference data. The acquired UAV DEM by UAV photogrammetry in February and May 2019, analyzes the volume change of Imlang beach and cross-shore profile analysis to survey the change of beach height. Finally, the shoreline is extract using the image segmentation technique of the high-resolution UAV orthomosaic in February and May 2019, respectively. The acquired shoreline analyzes the change (Fig. 1).

This study performed observations in February and May 2019 with the UAV photogrammetry to comprehensively evaluate the possibility of time-series coastal monitoring through the collected point clouds, orthomosaic and DEM.

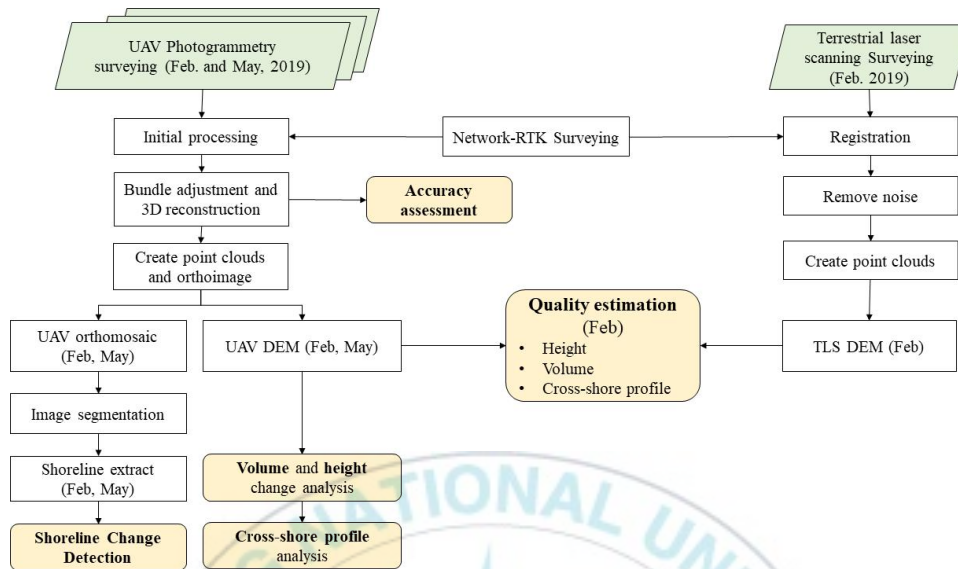


Fig. 2. Workflow in this study.

2. Methodology

2.1 Study area

The East Sea is characterized by a monotonous shoreline, compared with the West Sea and South Sea. It is constructed to local ports and coastal roads, shore protection in the area, along the long shoreline. It is caused the coastal erosion that construction of these structures (Hong, 2011). The east sea needs to research on coastal erosion.

The Korea Ministry of Ocean and Fisheries (KMOF) conducts annual coastal erosion monitoring in Busan coastal zone, classifying all the sandy beaches and uplands therein according to a four-grade system (A - D). coastal erosion monitoring results suggested that Imlang beach on the East Sea had a C-grade (concern) from 2014 to 2016. Recently Imlang beach have a B-grade (moderate) in 2017. Coastal erosion monitoring results indicate that Imlang beach is located in the southern part of the East Sea where coastal erosion is serious. Therefore, it is considered to be area that needs coastal monitoring, Imlang Beach was used as the study area. Imlang Beach is about 700 m long and 12 - 40 m wide. It is located at $35^{\circ}19'07''$ N and $129^{\circ}15'46''$ E. The main features of Imlang beach are exist about 70 m training dike on the left side and the right side of the Imlang port (Fig. 2).

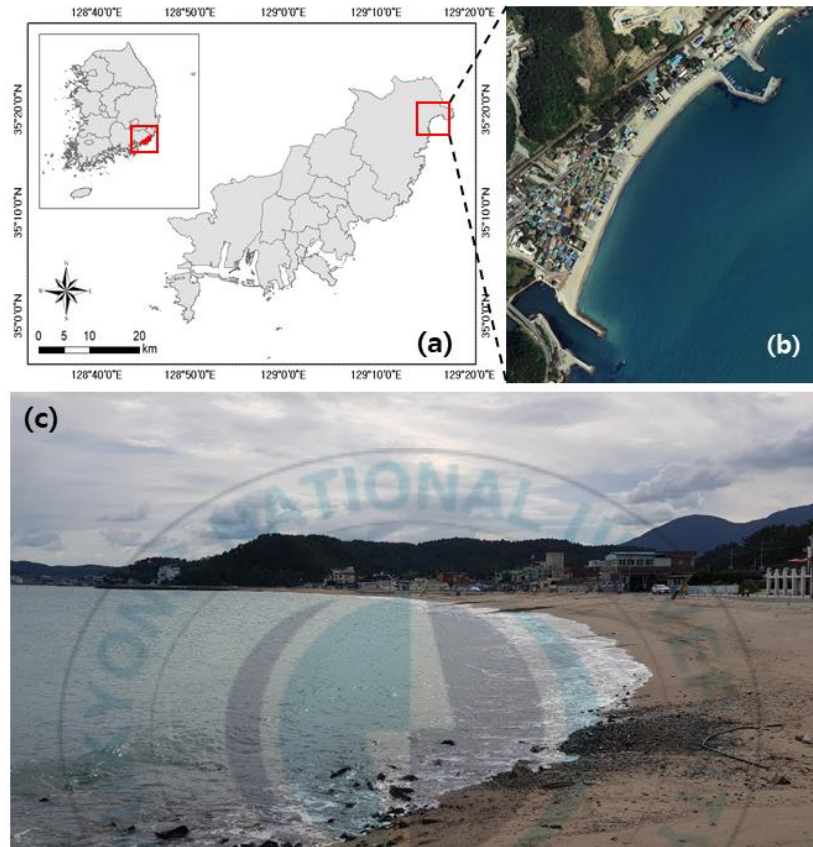


Fig. 3. The study area, (a) test field for this study is Imlang Beach in Busan, Korea, (b) aerial photographic in Imlang beach, (c) panoramic photographic in Imlang beach.

2.2 Data collection

2.2.1 UAV photogrammetry

UAV photogrammetry field campaigns were surveyed twice at Imlang beach in February and May 2019. UAV photogrammetry time

was chosen to coincide with low tide, large range of tide, so that the largest possible area can be mapped (Gonçalves and Henriques, 2015). Dates selected that satisfy conditions using the tidal tables published by KHOA. UAV photogrammetry time was chosen at 12:00–02:00 pm, when the sun position was centered. The reason is to minimize the occurrence of shadows and to avoid dark image collection in the acquired orthomosaic by UAV photogrammetry. UAV photogrammetry was surveyed at 12 pm on 25 February, and surveyed at 1 pm on 20 May.

DJI Inspire 2 UAV was used at Imlang beach in February and May 2019. Inspire 2 is the rotary wing of the Quadcopter, weight is 3.4 kg. maximum flight time is about 27 minutes and maximum flight speed is about 94 km/h. Inspire-2 is equipped with GPS and Inertial Measurement Unit (IMU), allowing hovering, automatic takeoff and landing, and attitude control.

The camera used Zenmuse X7 for UAV photogrammetry. Zenmuse X7 can be mounted on the Inspire 2. Zenmuse X7 size is $51 \times 108 \times 132$ mm, weight is 449 g, and Three-axis gimbal is $\pm 0.005^\circ$. Sensor image (still image) is 23.5×15.7 mm. Zenmuse X7 supports the Super 35 sensor, 24 mm lens and rolling shutter. Zenmuse X7 can also acquire $5,248 \times 3,936$ pixels images.

Pix4D Capture application was used to collect images of study area with UAV photogrammetry. Pix4D Capture application can be used to automatically capture the study area with multiple options such as pass-load, auto-pilot, frontlap, sidelap, altitude etc. Pix4D Capture application was set to the following options in this study, such as pass-load, altitude : 100 m, frontlap : 85%, sidelap : 75%, auto-pilot, velocity : 9.0 m/s (Fig. 3(a) and (b)). Pix4D Capture application options

were same setting by UAV photogrammetry in February and May 2019. Finally, the acquired number of images by UAV photogrammetry was 245 images in February and 240 images in May. Ground Sample Distance (GSD) was acquired at 1.59 cm in February and 1.62 cm in May.

The acquired images by UAV photogrammetry were processed using by Pix4D mapper ver 4.1.22 software (<https://www.pix4d.com>), in order to obtain the final result. Pix4D mapper software is based on the SfM algorithm, and conducts a total of three steps, (1) initial processing, (2) point clouds and mesh, (3) DSM, orthomosaic and index. The acquired UAV images and GCPs upload. GCPs surveyed by Network-RTK. Some of them are set to GCPs, to convert them to real coordinates. CPs is set to evaluate the absolute accuracy of the final model generated. The initial step is that UAV image conducts automatic matching and acquires corresponding keypoints from adjacent images. The keypoint can adjust the size of the image scale. In addition, exit orientation parameters are determined through the bundle adjustment. Next, dense point clouds are generated using the determined exterior orientation parameters and images by re-search the matching points. And it can create a mesh with a set of generated points. Finally, point clouds creates to triangulated irregular network (TIN). The produced TIN can be create DSM, orthomosaic (Kim and Kwon, 2019).

As a result, point clouds, orthomosaic were obtained in February and May 2019. The acquired spatial resolution of orthomosaic was 0.0159 m in February, and was 0.0162 m in May (Fig. 3(c) and (d)).

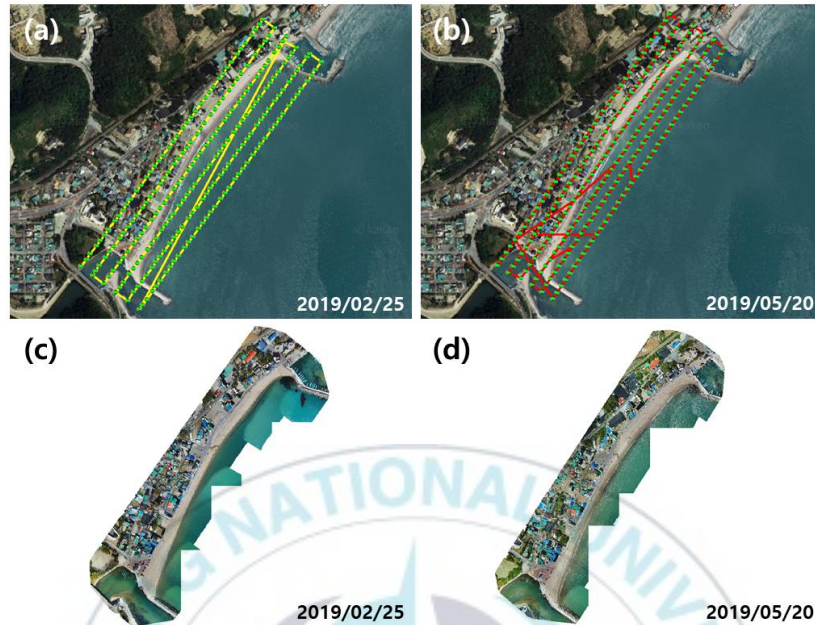


Fig. 4. UAV photogrammetry. UAV path on 25 February (a) and (b) UAV path on 20 May, UAV orthomosaic on 25 February (c), UAV orthomosaic on 20 May (d).

2.2.2 GNSS surveying

GCPs were surveyed using Network-RTK, before conducting UAV photogrammetry and terrestrial laser scanning (TLS) Surveying. The reasons for surveying GCPs are as follows. GCPs are required for image orientation, in the case of UAV photogrammetry (Goncalves and Henriques, 2015). Images through UAV photogrammetry are converted into a real coordinate system based on the 3-dimensional coordinates of GCPs using a triangulation method (Westoby et al., 2012). GCPs are used to assess accuracy as reference data (Jeong et al., 2018). TLS

surveying is conducted by the traverse method. 3-dimensional coordinates of selected traverse stations and upland sites are necessary for TLS based surveying (Mat zam et al., 2018) (Fig. 4(a)).

The used Network-RTK equipment was Sokkia GRX-2. Network-RTK used a set of options, such as UTM 52 zone coordinates of WGS-84 ellipsoid, HRMS 0.015, VRMS 0.030, epoch 30, antenna height 1.8 m.

For UAV photogrammetry, more than ten GCPs are needed to increase the accuracy of survey (Jeong, 2018; Rock et al., 2011). GCPs surveying by Network-RTK used artificial features such as manhole edges, angular edges of roadsides, and parking lot end line vertices in study area. Benchmarks installed on the beach. Network-RTK was surveyed forty GCPs in UAV photogrammetry February and was surveyed thirty-eight GCPs in UAV photogrammetry May (Fig. 4(b) and (c)). Network-RTK was surveyed twenty-two GCPs in TLS surveying February.

The acquired Network-RTK data was conducted to calibration using unified control point and benchmark. This is to construct accurate 3-dimensional coordinate Network-RTK data. The horizontal coordinate was corrected using three unified control points managed by the National Geographic Information Institute. The vertical coordinate was corrected using one benchmark operated by the KHOA (Fig. 5).

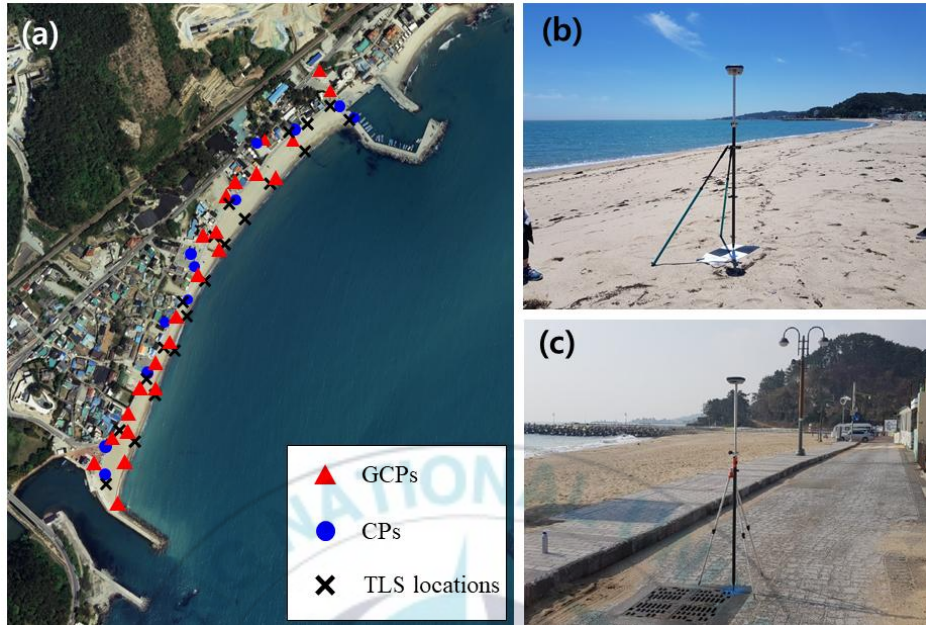


Fig. 5. Network-RTK surveying in study area. (a) Location of Network-RTK field campaign, (b) Network-RTK surveying on benchmark and (c) Network-RTK surveying on artificial feature.

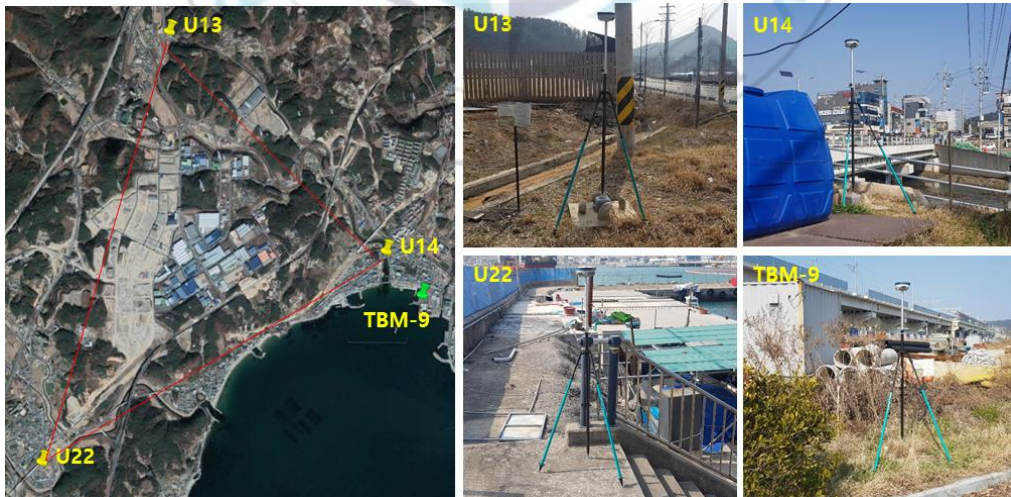


Fig. 6. Location of calibration data.

2.2.3 TLS laser scanning

TLS Surveying is a technique by injecting laser pulses to measure the time and wavelength of reach of the reflected laser. TLS Surveying is 3-dimensional point clouds of a station is obtained (Zang et al., 2019). TLS surveying provides high-density 3-dimensional terrain point clouds over a wide range of spatial scales. It is efficient and flexible method to rapidly capture high-precision 3-dimensional point clouds, for characterizing landscapes and monitoring geomorphological processes in coastal areas (Smith, 2016; Mat zam et al., 2018; Mancini et al., 2017; Zang et al., 2019). TLS surveying is an effective tool for detecting coastal topographical changes.

TLS surveying was conducted to collect density point clouds in the study area. The effectiveness of coastal monitoring of Imlang Beach was evaluated using UAV photogrammetry by comparing point clouds and DEMs constructed through TLS surveying

TLS surveying was conducted on February 25 2019. The used TLS equipment is Sokkia GLS-2000 in the study. This equipment offers significant advantages in terms of scanning velocity, point interval and resolution (Mat zam et al., 2018). It has a maximum pulse range of 500 m, maximum scanning velocity is 120,000 point/s, and weight is about 11 kg. Sokkia GLS-2000 is deployed to survey the entire study area at Imlang beach. It is conducted to option that scan interval was 12.5 mm at 10 m, and scan mode was set to regular (Fig. 6(a) and (b)). TLS surveying time was consumed about 8 hours from 9:00 am to 5:30 pm. TLS surveying was conducted on the coastal roads and the interior of the beach where surveyed data by Network-RTK (Fig. 6(c)). Acquired

21 station data were registered by Scan-master software. (<https://www.topcon.co.jp>). The collected point clouds at all 21 stations were merged into a single point cloud using a registration process. Merged point clouds are totally 79,398,901. The average positional error of occupation and backsight by station indicated -0.004 m, -0.004 m, -0.002 m in the X, Y and Z direction, respectively (Table 1). All points outside of Imlang Beach were eliminated that noise, structure etc from the merged point cloud. The final point cloud acquired 58,874,026 points (Fig. 6(d)).

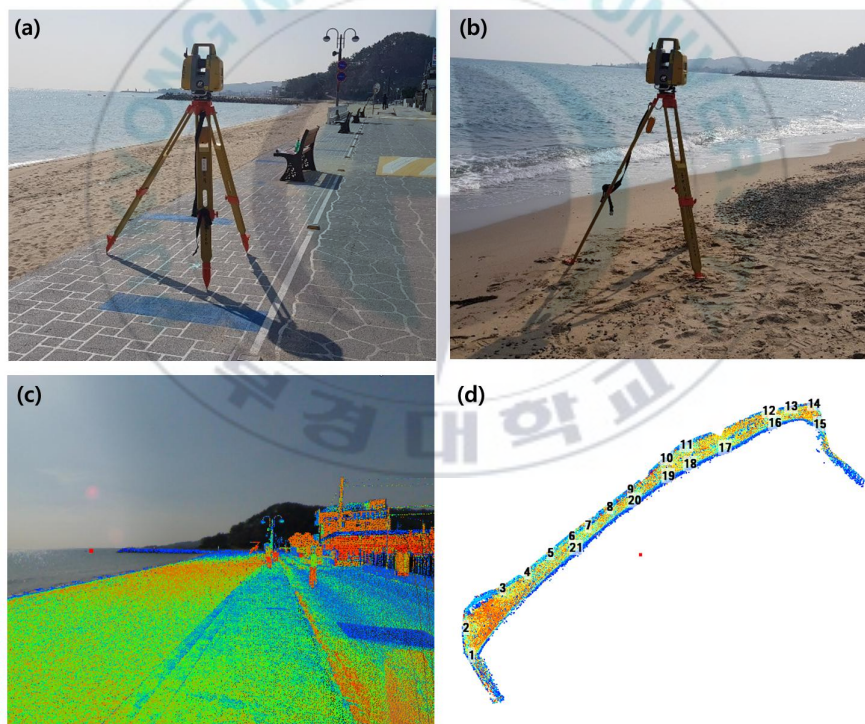


Fig. 7. TLS surveying in study area. (a) TLS surveying on the road and (b) TLS surveying on the beach, (c) station view, (d) acquired point clouds.

Table 1. Orientation error for each TLS station (unit: m)

Station	Dx	Dy	Dz	Station	Dx	Dy	Dz
1	0.002	-0.003	-0.007	12	0.001	0.001	-0.028
2	0.014	0.039	-0.008	13	0.011	0.006	0.028
3	0.022	0.032	0.027	14	0.000	0.000	-0.029
4	-0.010	-0.021	-0.036	15	-0.014	0.001	-0.008
5	0.001	0.002	-0.007	16	-0.027	-0.033	-0.013
6	-0.013	-0.002	-0.001	17	-0.062	-0.069	0.015
7	0.004	0.009	0.023	18	-0.004	-0.005	0.025
8	0.011	0.022	0.034	19	-0.013	-0.022	-0.026
9	0.019	0.004	-0.039	20	-0.027	-0.05	-0.009
10	0.011	0.017	0.007	21	0.002	0.002	0.014
11	-0.018	-0.028	-0.007	Mean	-0.004	-0.004	-0.002



3. Results and Discussion

3.1 Accuracy assessment

The acquired images by UAV photogrammetry were processed using Pix4D mapper software based on SfM algorithm to acquired final data. Bundle adjustments are performed during Pix4D mapper software initial processing to connect the corresponding image point and the center of projection of the image according to the input ground reference point. The acquired UAV image is generated as the final data through the bundle adjustment process. The accuracy of the generated UAV data can be verified by comparing the GCPs coordinates from the input GCPs coordinates and the final data generated by the UAV photogrammetry (Choi and Lee, 2016). The position difference at the same point between the previously manually set GCPs and the final set results GCPs indicates the positional accuracy quality. The positional accuracy of coordinates can be expressed in RMSE and can be used in Pix4D mapper software (Mölg and Bolch, 2017). It can also evaluate the absolute accuracy of the generated data by setting CPs through random selection of acquired GCPs (Choi and Lee, 2016).

The quality of positional accuracy affects the accuracy of the UAV photogrammetry result, depending on altitude, frontlap, sidelap, the number of GCPs (Long et al., 2016). Many researchers evaluated the location accuracy of the UAV result based on the presence of GCPs as well as altitude, frontlap, sidelap, and the number of GCPs. Yoo et al. (2016) assessed the positional accuracy quality according to the

frontlaps, sidelaps and number of GCPs at altitude 160m, as a result of the UAV photogrammetry performance. In case of three GCPs, the horizontal accuracy was 0.046 m, 0.054 m, 0.045 m, and the vertical accuracy was 0.189 m, 0.114 m, 0.095 m; frontlap and sidelap are 50/60, 60/70, 70/80, respectively. The horizontal accuracy was 0.040 m, 0.046 m, 0.040 m, and the vertical accuracy was 0.154 m, 0.123 m, and 0.064 m for six GCPs. Yanagi et al. (2016) evaluated the positional accuracy quality according to the number of GCPs for altitude 50 and 100 m for images collected with UAV photogrammetry using a Pix4D mapper software. The horizontal accuracy was 0.042 m, and the vertical accuracy was 0.087 m for at least three GCPs at altitude 50 m. The thirteen GCPs were found to be 0.035 m and 0.060 m. The difference between the three GCPs and thirteen GCPs in RMSE was 0.007 m for the horizontal accuracy and 0.013 m for the vertical accuracy. The thirteen GCPs horizontal and vertical accuracy were 0.077 m and 0.092 m. The difference between three GCPs and thirteen GCPs in RMSE was 0.015 m for the horizontal accuracy and 0.021 m for the vertical accuracy. Long et al. (2016) performed a positional accuracy assessment according to height using nineteen GCPs at approximately 65 and 150 m altitude. It was reported that RMSE was 0.016 m, 0.016 m, 0.016 m in the X, Y and Z direction, respectively when altitude was about 150 m. and 0.012 m, 0.012 m, 0.012 m in the X, Y and Z direction, respectively when altitude was about 65 m. This means that the positional accuracy assessment is affected by altitude. Muji and Tahar. (2017) performed UAV accuracy assessment of the existence of GCPs, in addition to bundle adjustment accuracy assessment based on the above mentioned option of altitude, frontlap, sidelap and number of GCPs. A positional accuracy assessment was performed for GCPs using

Pix4D mapper software for data collected through the UAV photogrammetry at altitude 100 m. RMSE in the absence of GCPs was shown at 7.90 m, 19.64 m and 17.92 m in the X, Y and Z direction, respectively, and RMSE with GCPs was 0.68 m, 0.69 m, 0.37 m in the X, Y and Z direction, respectively. In the previous study, it was found that positional accuracy affected the bundle adjustment accuracy according to altitude, frontlap, sidelap, and the number of GCPs.

UAV photogrammetry was performed at altitude 100 m, frontlap 75%, and sidelap 85% in the study area. thirty-eight Network-RTK observations were used, 25 of which were set to GCPs for the UAV photogrammetry in February. The rest thirteen were set to CPs to evaluate the absolute accuracy of the generated data. As a results of the UAV photogrammetry processing conducted in February showed that RMSE for February GCPs, which indicates the positional accuracy of the generated data, was 0.010 m, 0.008 m, 0.016 m in the X, Y, and Z directions, respectively. The UAV photogrammetry carried out in May used 38 GCPs as in February, with GCPs and CPs selecting the same point as in February. As a result, RMSE for GCPs was 0.012 m, 0.011 m, 0.018 m in the X, Y, and Z directions in May (Table 2). Whereas for RMSE of CPs, which indicates the absolute accuracy of the generated data was 0.015, 0.017, 0.040 in the X, Y, and Z directions in February, respectively. RMSE for CPs was 0.018 m, 0.015 m, and 0.035 m in the X, Y, and Z directions in May, respectively (Table 3).

We compared the positional accuracy of UAV photogrammetry derived from this study and the results performed with the same altitude in other studies. Papakonstantinou et al. (2016) performed UAV photogrammetry at altitude 100 m, in Eressos beach and Neapolis beach. The location accuracy of the Eressos beach was 0.041 m, 0.039

m, 0.004 m in the X, Y and Z direction, respectively, and Neapolis beach 0.105 m, 0.046 m, and 0.028 m in the X, Y and Z direction, respectively. Jeong et al. (2018) was set up similar to the flight option set in this study, and measurements showed that RMSE for height was 0.036 m. Comparing with the results of this study, it can be found that RMSE for X and Y performed better than that of Papakonstantinou et al. (2016) and that RMSE results for Z were derived lower. Jeong et al. (2018) RMSE results similar to the study appeared. The difference of error for each scale in the Korean Public Survey Regulation using UAV is horizontal ± 0.2 m, vertical ± 0.2 m for 1/5000. As a result of comparison with this study, it indicated the position accuracy that satisfies the unmanned aerial survey work regulation.

Table 2. RMSE statistics by 25 ground control points (unit: m)

	X	Y	Z
February, 2019	0.010	0.008	0.016
May, 2019	0.012	0.011	0.018

Table 3. RMSE statistics by 13 check points (unit: m)

	X	Y	Z
February, 2019	0.015	0.017	0.040
May, 2019	0.018	0.015	0.035

3.2 Quality estimation

The dense 3-dimensional point clouds in February and May 2019

were produced using Pix4D mapper software. The number of point clouds in February and May were acquired 28,008,133 and 26,306,592, and the an average densities were calculated to be 559 per m³ and 580 per m³, respectively. Point clouds that correspond to structures on the beach and point clouds other than the beach were removed in order to calculate the precise area and volume in the beach. Because the shape and size of the stream changed significantly between February and May. Also errors about the height value was indicated. The stream, which across the beach, was also removed.

The number of points in modified point clouds were acquired 2,740,881 and 2,756,792. The average densities were calculated to be 253.01 per m³ and 253.31 per m³ in February and May, respectively. The number of points and an average density were calculated to be 21,006,915 and 1,930.25 per m³ in TLS point clouds.

The DEM was produced using point clouds with 3-dimensional spatial information to calculated the volume of the beach (Jansen, 2018). The point clouds of TLS, UAV in February and May were used to generate three DEMs with 0.016 m spatial resolution using Inverse Distance Weighted (IDW) interpolation method. The spatial resolutions of UAV orthomosaic also were set 0.016 m for high resolution image analysis in February and May, respectively.

TLS DEM was selected as the reference data in order to validate the collected DEM through UAV photogrammetry. The maximum height of the TLS DEM and UAV DEM is 3.96 m and 3.96 m, and the minimum height is 0.89 m and 0.91 m, respectively. The maximum height of UAV DEM was 3.91 m and the minimum height was 0.81 m in May (Fig. 7). The height comparison of the TLS DEM and the UAV DEM, the area analysis presented that the area of the TLS DEM and

the UAV DEM was equally calculated to be 10,883.02 m². The volume of TLS DEM and UAV DEM in February was calculated 26,851.88 m³, and 27,039.02 m³. The difference of two volumes was calculated to be 0.7% (Table 4). The average height difference and RMSE of DEM by TLS and UAV were calculated ± 0.017 m and 0.032 m. Cross-shore profile analysis was performed using CS provided by MOF to analyze the height difference between TLS DEM and UAV DEM (Fig. 8). Six CSs were selected for analysis, the minimum heights of six CSs were calculated 0.001–0.024 m and the highest difference was presented 0.024 m in the fourth CS of six CSs. In case of the maximum heights were calculated 0.061–0.104 m, in particular, the maximum height was presented 0.104 m in the first CS (Table 5). For the first CS, it is believed that there is a road that can enter the beach, resulting in maximum value as many people pass by.

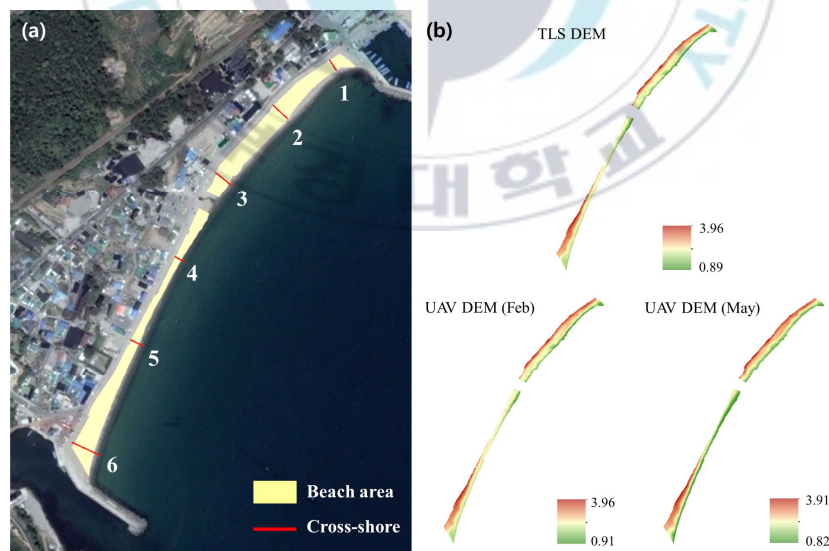


Fig 8 Marking the location of the data to be used in the study. (a) Beach area and cross-shore and (b) DEM derived from UAV photogrammetry and TLS surveying.

In others study, which studied about validation between UAV and traditional surveying techniques, Niethammer et al. (2012) verified RMSE of 0.31 m between DEM acquired by UAV photogrammetry and DEM based on TLS at altitude 100–200 m. A lot of studies verified the result of UAV photogrammetry using GNSS data as reference data. Mancini et al. (2013) also verified the UAV DEM and TLS DEM acquired at altitude 40 m using GNSS data, RMSE value calculated 0.011 m. Harwin and Lucieer. (2012) presented that RMSE of height calculated 0.025–0.04 m between the result of UAV photogrammetry and the result of DGPS at altitude 50 m. Udin and Ahmad (2012) calculated 0.639 m RMSE between the result of UAV photogrammetry and the result of GNSS data at altitude 100 m.

Table 4. Comparison of volumes between TLS DEM and UAV DEM in February

	Points	Area (m ²)	Point density (point/m ²)	Volume (m ³)	Volume difference (%)
TLS	21,006,915	10,883.02	1,930.25	26,851.879	0.7
UAV (Feb)	2,740,881	10,883.02	253.01	27,039.022	

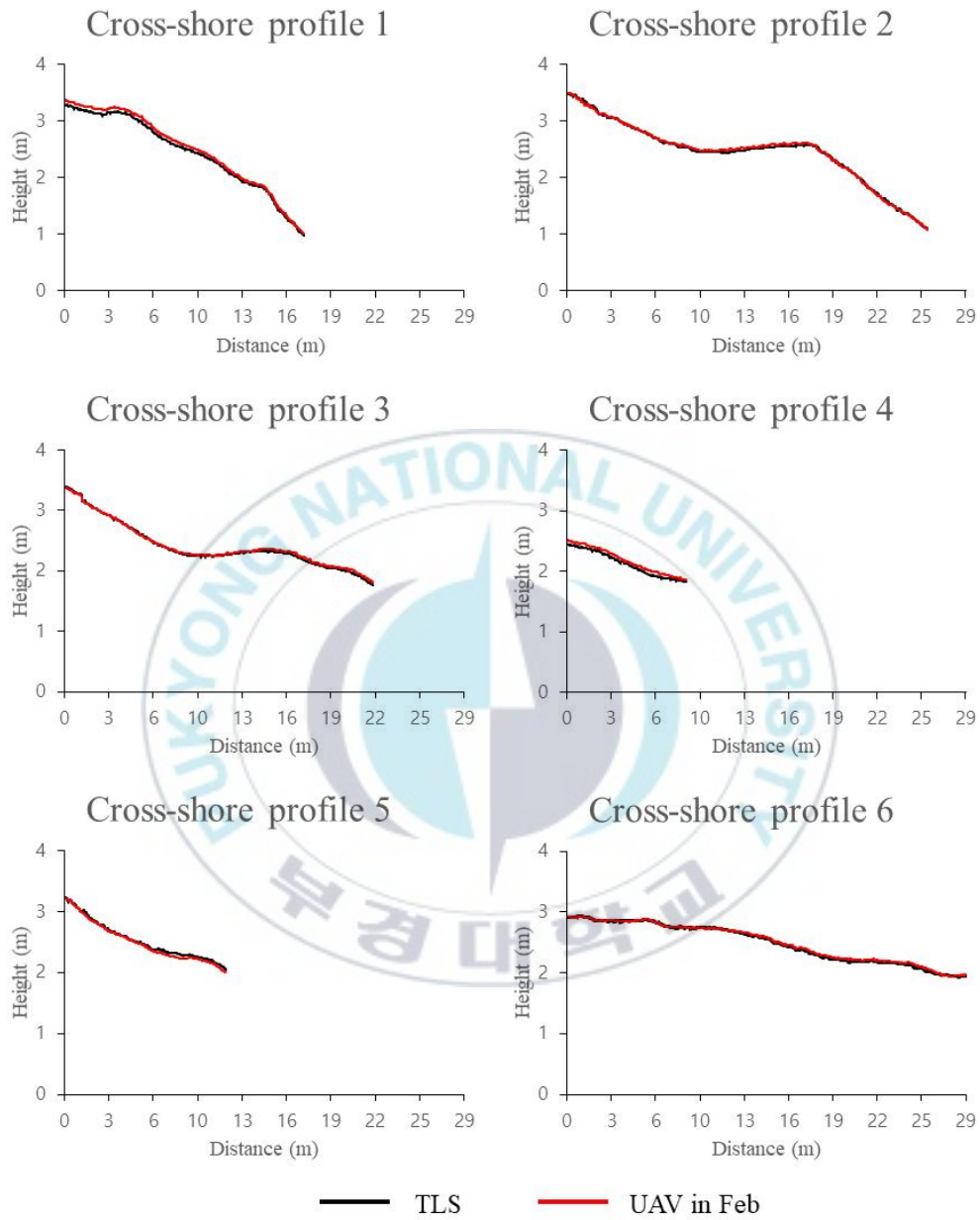


Fig. 9. Graph of cross-shore profiles between UAV photogrammetry in February (red) and TLS surveying (black).

Table 5. Difference of vertical between TLS DEM and UAV DEM in February (Unit: m)

	CS 1	CS 2	CS 3	CS 4	CS 5	CS 6
Min	0.001	0.001	0.001	0.024	0.001	0.001
Max	0.104	0.078	0.067	0.085	0.078	0.061
Mean	0.059	0.024	0.022	0.056	0.031	0.016

3.3 Beach vertical change detection

Cross-shore profile is also useful tool for monitoring spatial and periodic long-term trends such as coastal erosion, and for predicting changes in coastal topography (Dora et al., 2012). Cross-shore profiles were produced to analysis coastal topography using CS collected by UAV DEM. After overlaid the collected DEM by UAV in February and May (Fig. 9), cross-shore profiles analysis were performed using six CS provided by coastal portal (coast.mof.go.kr) of MOF. The results of minimum difference were calculated 0.001–0.270 m in February and May. The difference of fourth CS presented that the highest height. In case of the results of maximum difference were calculated 0.274–1.058 m, in particular, the difference of 5th CS presented the highest height. The average distribution of each CS was calculated 0.098–0.750 m, the fourth CS presented the maximum distribution and the first CS presented the minimum distribution (Table 6). The difference of average height in UAV DEM was calculated 0.165 m in February and May. The difference of volume was calculated about 6.6% (Table 7).

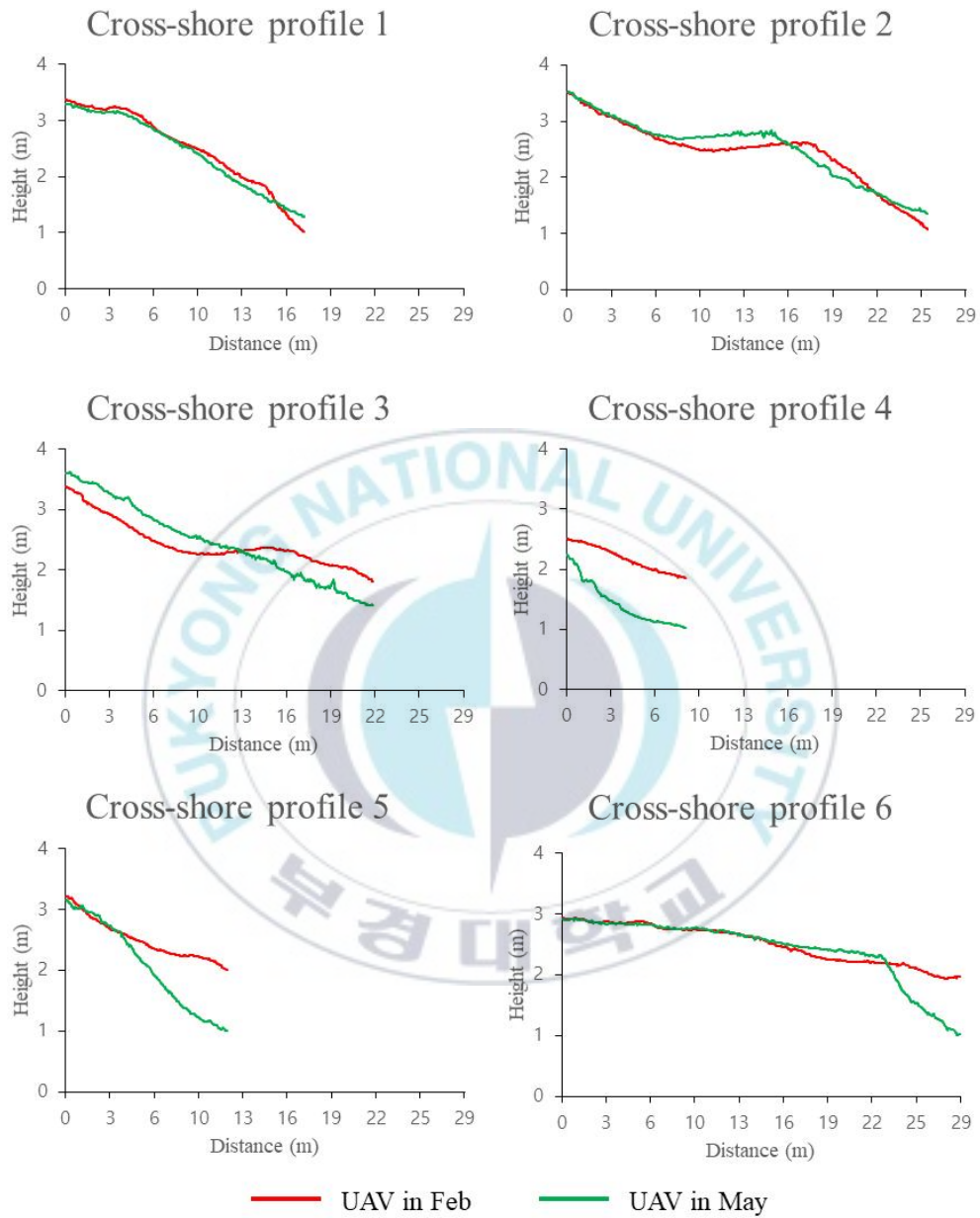


Fig. 10. Graph of cross-shore profiles between UAV photogrammetry in February (red) and UAV photogrammetry in May (green).

Table 6. Difference of vertical between UAV DEM in February and May (Unit: m)

Line	CS 1	CS 2	CS 3	CS 4	CS 5	CS 6
Min	0.001	0.001	0.001	0.270	0.001	0.001
Max	0.274	0.324	0.506	0.889	1.058	0.957
Mean	0.098	0.135	0.303	0.750	0.451	0.149

Table 7. Comparison of volume by UAV DEM in February and May

	Points	Area (m ²)	Point density (point/m ²)	Volume (m ³)	Volume difference (%)
UAV (Feb)	2,740,881	10,883.02	253.01	27039.022	6.6%
UAV (May)	2,756,792	10,883.02	253.31	25242.647	

The 3rd, 4th, and 5th in Cross-shore profile shows more height the other CSs. The 3rd CS is located around the stream which formed tidal channel, because the topography and shape of the tidal channel changes between February and May. It seems to have influenced 3rd CS.

There is a road that can enter the beach near 3rd CS. This road was being expanded to near 3rd CS in May (Fig. 10(a) and (b)). Coastal roads were under construction as part of the coastal maintenance project during UAV photogrammetry surveying in 20 May in case of 4th CS and 5th CS. Therefore, these artificial construction seems to have changed the coastal erosion rapidly (Fig. 10(c) and (d)).

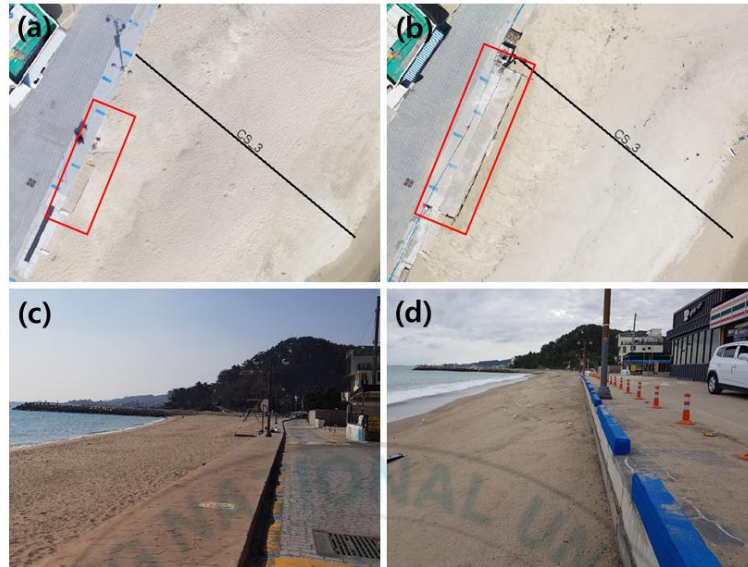


Fig. 11. Before and after beach construction in the study area. (a) before beach road construction, (b) after beach road construction and (c) before sidewalk road construction, (d) after beach sidewalk road construction.

3.4 Shoreline detection with image segmentation

Geographic Object-Based Image Analysis (GEOBIA) based on geographic objects was used to the acquired high-resolution orthomosaic by UAV photogrammetry in order to extract the shoreline of Imlang beach. GEOBIA has been applied in many ocean applications such as shoreline and beach zone detection (Papakonstantinou et al., 2016; Topouzelis et al., 2017). Shoreline was extracted from UAV orthomosaic using image segmentation technique to group pixels with similar spectrum and spatial characteristics in this study. (Papakonstantinou et al., 2016). To perform image segmentation of UAV orthomosaic, a multiresolution segmentation algorithm of eCognition

Developer 9.0 software used. Multiresolution segmentation conducts merging and splitting to segment similar pixels in UAV orthomosaic. This process is divided into geographic objects through homogeneity criterion of color, shape, compactness, smoothness. Multiresolution segmentation parameters are classified into various sizes according to shape, compactness, smoothness values (Yang and Hwang, 2012). The result produce a homogeneous image object for different types of data (Baatz and Schäpe, 2010). The homogeneous image objects were produced for different types of data (Baatz and Schäpe, 2010). Finally, geographic objects were divided and clustered into homogeneous areas (Darwish et al., 2003).

The setting of multiresolution parameters is important. Yang and Hwang. (2012) reported that it is necessary to find appropriate standards or methods through trial and error, because the parameter of multiresolution segmentation is difficult to explain clearly the relationship between image segmentation results.

Ventura et al. (2018) reported that size value of the multiresolution segmentation parameters is appropriate between 100 and 150 when using multiresolution segmentation for high resolution UAV orthomosaic. The multiresolution segmentation parameter size is set to 100 in this study. Shape and compactness parameters can be set in the range of 0.1-0.9. Moon et al. (2017) reported that although the segmented images were generated by applying the shape, compactness parameters sequentially in units of 0.1, shape and compactness did not change significantly between 0.1 and 0.5. Shape and compactness parameters were applied equal to 0.5. Image segmentation was conducted in this study. The same parameter was applied to the acquired high-resolution orthomosaic using UAV photogrammetry at Imlang beach in February

and May, respectively. Wetlands and dryland can be classified using thresholds that mean RGB values, mean brightness, standard deviation RGB, position, shape in segmented images. Wetlands and drylands were classified using mean RGB values in this study. the mean RGB threshold of 165 was used in UAV orthomosaic February, and the mean RGB threshold of 167 was used in UAV orthomosaic May (Fig. 11(a) and (b)).

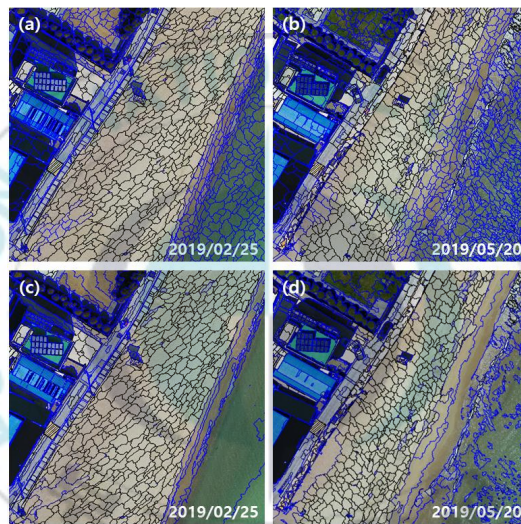


Fig. 12. Image segmentation. (a) Multiresolution segmentation on 25 February, (b) multiresolution segmentation on 20 May and (c) spectral difference segmentation on 25 February, (d) spectral difference segmentation on 20 May.

The classified segmentation images by mean RGB threshold were merged with adjacent objects using spectral difference segmentation. Spectral difference segmentation is an algorithm that merges adjacent objects below a given threshold in a previously segmented orthomosaic. Wetland and dryland were merged by similar thresholds (Fig. 11(c) and

(d). The merged wetlands and drylands were partially merged, not completely, only the wetlands were merged. Finally, only merged wetlands were acquired to use shoreline as vectors in February and May, respectively (Fig. 12).



Fig. 13. The acquired shoreline in February and May.

3.5 Shoreline change analysis

The changes of shoreline were analyzed by digital shoreline analysis system (DSAS) 4.3 ver program. The DSAS program calculates the rate of change for the acquired shoreline by constructing a baseline directly adjacent to the shoreline (Thieler et al, 2009). The used data for the analysis of shoreline change is a baseline which the boundary between beach and land, and shorelines in February and May 2019,

respectively. The baseline can be constructed by user (Thieler et al, 2009). A total of 66 transects with 100 m-long at 10 m intervals, based on the baseline, were produced for shoreline analysis (Fig. 13).

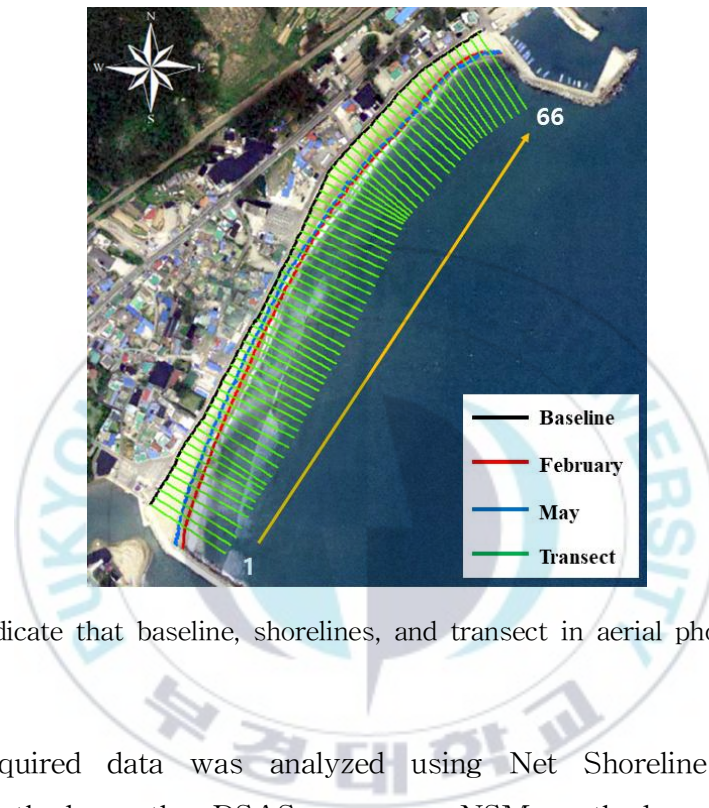


Fig. 14. Indicate that baseline, shorelines, and transect in aerial photographic.

The acquired data was analyzed using Net Shoreline Movement (NSM) method on the DSAS program. NSM method represents the total distance between the oldest and most recent shoreline (Thieler et al., 2009; Lee et al., 2013). As a result of NSM analysis, it was indicated minimal advance in transect No. 65, about +0.89 m. Also, transect No. 57 was indicated maximum advance about 4.85 m. On the other hand, transect No. 4 indicated maximum retract was about -10.08 m. Transect No. 51 indicated the minimum retreat was about -1.16 m. The retreat toward land is - and the advance toward sea is + (Fig. 14).

Analysis results indicated that transect No. 54-66 was the advance shoreline, with an average rate of change of 2.38 m. Transect No. 1-53 was the retreat shoreline, with an average rate of change of -5.54 m. This change in February and May means that transect No. 1-53 retreat northwest, and transect No. 54-66 advance southeast.

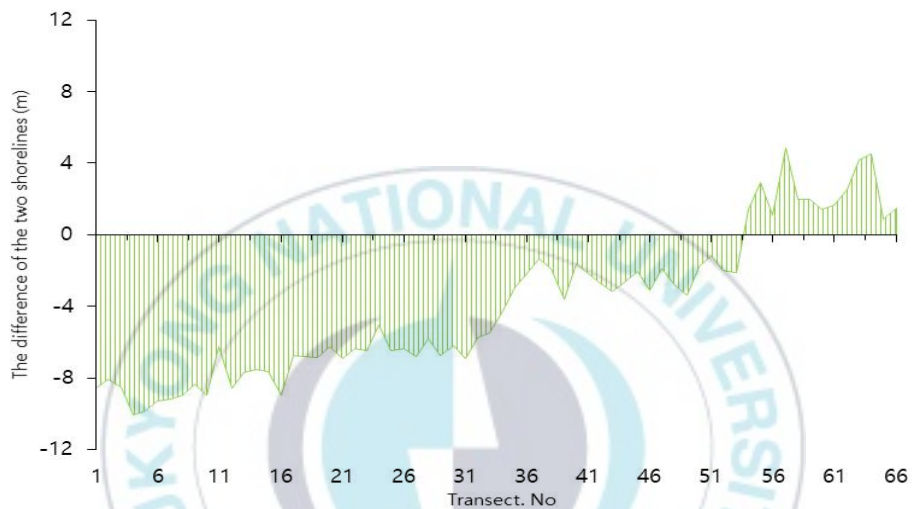


Fig. 15. Graph of shoreline change.

4. Conclusions

The possibility for coastal monitoring based on UAV photogrammetry is presented in this study. The volume change detection is provided from the acquired UAV DEM. This provides information on vertical variation based on cross-shore profile data from collected UAV data. It is also valuable for the detection of shoreline and for the observation of changes in UAV orthomosaic.

The UAV photogrammetry were conducted at 100 m altitude at Imlang beach in February and May, respectively. It acquired 245 images with the GSD 1.59 in February and 240 images with the GSD 1.62 in May. We evaluated RMSE accuracy estimates for X, Y, and Z direction of the UAV results using twenty-five GCPs and thirteen CPs obtained through Network-RTK. The results showed that RMSE was 0.015, 0.017, 0.040 m in the X, Y and Z direction in February, and RMSE was 0.018, 0.015, 0.035 m in the X, Y and Z direction in May, respectively. The high-density 3-dimensional point clouds were created by applying SfM algorithm to UAV images using Pix4D Mapper. The accuracy of the generated UAV DEM was assessed using the acquired high density point clouds through TLS surveying. The average height difference between UAV DEM and TLS DEM was 0.017 m and RMSE was 0.032 m. The average volume of DEM generated by UAV photogrammetry DEM and TLS surveying is about 0.7%, which means there is no significant difference. The difference in average volume of UAV DEM in February and May was about 6.6%. In addition, six CSs were generated and analyzed to check the difference in vertical variation for the UAV DEM at Imlang beach in February and May. As a result, UAV photogrammetry provided accurate vertical variation data.

The analysis of the cross-share profile indicated that there were many changes in 3rd, 4th, and 5th CSs at Imlang beach. This may be due to coastal roads, sidewalk expansion, coastal ramp extension as part of the coastal maintenance project in the early May. As a result, UAV photogrammetry was confirmed to provide accurate vertical variation data.

Finally, the GEOBIA method was applied to high resolution orthomosaic images to extract the shoreline of the Imlang beach, using eCognition Developer 9.0 software. The wetland and dryland were classified by applying threshold to the average RGB value. The Spectral Differentiation Segmentation algorithm was applied to the classified images to perform clustering of wetland, and then merged the vector corresponding to wetland to collect the shorelines in February and May respectively. NSM was used to analyze acquired shoreline changes. NSM represents the total distance between the oldest shoreline and the most recent shoreline. As a result, on the based transect No. 54, the shoreline was advanced in the sea orientation in transect No. 54-66. The shoreline was retreated in the land orientation in transect No. 1-53.

The UAV photogrammetry method is more efficient than other equipment in terms of time and cost when performing coastal monitoring tasks. It took about 8 hours to collect reference data using TLS surveying, while 10 minutes were spent using UAV photogrammetry. As a result, point clouds, DEM, and orthomosaic acquired through UAV photogrammetry are accurate and are a convenient way to provide sufficient quality data for continuous coastal monitoring.

References

- Alesheikh, A.A., Ghorbanali, A., & Nouri, N. (2007). Coastline change detection using remote sensing, *International Journal of Environmental Science & Technology*, 4(1): 61-66.
- Baatz, M., & Schäpe, A. (2010). Multiresolution segmentation: an optimization approach for high quality multi-scale image segmentation. 2000, URL: http://www.agit.at/papers/2000/baatz_FP_12.pdf.
- Casella, E., Rovere, A., Pedroncini, A., Mucerino, L., Casella, M., Cusati, L. A., Vacchi, M., Ferrari, M. and Firpo, M. (2014). Study of wave runup using numerical models and low-altitude aerial photogrammetry: A tool for coastal management, *Estuarine, Coastal and Shelf Science*, 149: 160-167.
- Casella, E., Rovere A., Pedroncini A., Stark C. P., Casella M., M. Ferrari M and Firpo M. (2016). Drones as tools for monitoring beach topography changes in the Ligurian Sea (NW Mediterranean), *Geo-Marine Letters*, 36(2): 151-163.
- Choi, K.A. & Lee, I.P. (2016). Accuracy analysis of coastal area modeling through UAV photogrammetry, *Korean Journal of Remote Sensing*, 32(6): 657-672.
- Darwish, A., Leukert, K., & Reinhardt, W. (2003). Image segmentation for the purpose of object-based classification, *IGARSS 2003. 2003 IEEE International Geoscience and Remote Sensing Symposium. Proceedings (IEEE Cat. No. 03CH37477)*, vol. 3, pp. 2039-2041.

- Defeo, O., McLachlan, A., Schoemanm D.S., Schlacher, T.A., Dugan J., Jones, A., Lastra, M. & Scapini, F. (2009). Threats to sandy beach ecosystems: a review, *Estuarine, Coastal and Shelf Science*, 81(1): 1-12.
- Dora, G.U., Kumar, V.S., Johnson G., Philip, C.S., & Vinayaraj, P. (2012). Short-term observation of beach dynamics using cross-shore profiles and foreshore sediment, *Ocean & Coastal Management*, 67: 101-112.
- Douglas, B.C., & Crowell, M. (2012). Long-term shoreline position prediction and error propagation, *Journal of Coastal Research*, 16(1).
- Drummond, C.D., Harley, M.D., Turner I.L., Matheen, A.N.A. & Glamore, W.C. (2015). UAV applications to coastal engineering, *Australasian Coasts & Ports Conference 2015: 22nd Australasian Coastal and Ocean Engineering Conference and the 15th Australasian Port and Harbour Conference*, pp. 267.
- Gonçalves, J., & Henriques, R. (2015). UAV photogrammetry for topographic monitoring of coastal areas, *ISPRS Journal of Photogrammetry and Remote Sensing*, 104: 101-111.
- Guillot, B., Castelle, B., Marieu, V., Bujan S., & Rosebery, D. (2018). UAV monitoring of 3-year Foredune Partial Recovery from a Severe Winter: Truc Vert Beach, SW France, *Journal of Coastal Research*, 85(sp1): 276-280.
- Harwin, S., & Lucieer, A. (2012). Assessing the accuracy of georeferenced point clouds produced via multi-view stereopsis from unmanned aerial vehicle (UAV) imagery, *Remote Sensing*, 4(6): 1573-1599.

- Holman, R.A., & Stanley, J. (2007). The history and technical capabilities of Argus, *Coastal Engineering*, 54(6-7): 477-491.
- Hong, D.H. (2011). Coastal Managements and Restoration Works for Beach Erosion on the East Coast of Korea. Catholic Kwandong University
- Jansen, K.M. (2018). Analysis of photogrammetric mapping using low-cost unmaned aerial vehicle in coastal areas
- Jeong, E., Park, J.Y., & Hwang, C.S. (2018). Assessment of UAV Photogrammetric Mapping Accuracy in the Beach Environment, *Journal of Coastal Research*, 85(sp1): 176-180.
- Jeong, S.J. (2018). Development of Image Preprocessing Techniques and Fresh Weight Estimation Models for Onion (*Allium cepa*) and Garlic (*Allium sativum*) using UAV-Image Sensors. Seoul National University
- Jiménez López, J., & Mulero-Pázmány, M. (2019). Drones for conservation in protected areas: present and future, *Drones*, 3(1): 10.
- Kim, H.J. (2015). Beach Surveying and Littoral Current Observation using UAV. Jeonnam National University
- Kim, J.S., Lee, S.K., Ahn, H.Y., Seo, D.J., Seo, D.C., Lee, J.C. and Choi, C.U. (2013). Accuracy evaluation of a smartphone-based technology for coastal monitoring, *Measurement*, 46(1): 233-248.
- Kim, Y.G., & Kwon, J.W. (2019). The Maintenance and Management Method of Deteriorated Facilities Using 4D map Based on UAV and 3D Point Cloud. *Journal of the Korea Institute of Building Construction*, 19(3), 239-246
- King, S., Leon, J., Jackson, M.L. & Corbett, B. (2017). Condition survey of coastal structures using UAV and photogrammetry, *Australasian*

- Coasts & Ports 2017: Working with Nature: 704.
- Laidlaw, S. (2017). Unmanned Aerial System (UAS) and Structure From Motion (SfM) 3-dimensional modeling of intertidal archaeological features in Fulford Harbour, Saltspring Island, British Columbia, Canada.
- Lee, G.S., Choi, Y.W. & Lee, J.H. (2016). Building of 3D Terrain Modeling and Evaluation of Location Accuracy using UAV in Beach Area, Journal of the Korean Cadastre Information Association, 18(2): 207-216.
- Lee, G.W., Son, H.U., Kim, D.I. (2017). Drone remote sensing photogrammetry
- Lee, J.O., Kim, Y.S., Park, S.B. & Park, C.Y. (2013). The Analysis of Eulsukdo Shoreline Change Using Multi-temporal Aerial Photo And DSAS Program, Journal of Korean Society for Geospatial Information System, 21(1): 11-18.
- Lee, K.S., Choi, J.M. & Joh, C.H. (2015). Method to extract coastline changes using unmanned aerial vehicle, The Korean Geographic Society, 50(5): 473-483.
- Li, X. & Damen, M. C. (2010). Coastline change detection with satellite remote sensing for environmental management of the Pearl River Estuary, China, Journal of Marine Systems, 82: S54-S61.
- Lomax, A., Corso, W. & Ebro, J. (2005). Employing unmanned aerial vehicles (UAVs) as an element of the Integrated Ocean Observing System, Proceedings of OCEANS 2005 MTS/IEEE, pp. 184-190.
- Long, N., Millescamp, B., Guillot, B., Pouget F. & Bertin, X. (2016). Monitoring the topography of a dynamic tidal inlet using UAV imagery, Remote Sensing, 8(5): 387.
- Long, N., Millescamp, B., Pouget F., Dumon, A., Lachaussée N. &

- Bertin, X. (2016). Accuracy assessment of coastal topography derived from UAV images, *The International Archives of Photogrammetry, Remote Sensing and Spatial Information Sciences*, 41: 1127.
- Maglione, P., Parente, C. & Vallario, A. (2014). Coastline extraction using high resolution WorldView-2 satellite imagery, *European Journal of Remote Sensing*, 47(1): 685-699.
- Mancini, F., Castagnetti, C., Rossi, P., Dubbini, M., Fazio, N., Perrotti, M. & Lollino, P. (2017). An integrated procedure to assess the stability of coastal rocky cliffs: From UAV close-range photogrammetry to geomechanical finite element modeling, *Remote Sensing*, 9(12): 1235.
- Mancini, F., Dubbini, M., Gattelli, M., Stecchi, F., Fabbri, S. & Gabbianelli, G. (2013). Using unmanned aerial vehicles (UAV) for high-resolution reconstruction of topography: The structure from motion approach on coastal environments, *Remote Sensing*, 5(12): 6880-6898.
- Martínez, M. L., Intralawan, A., Vázquez, G., Pérez-Maqueo, O., Sutton P. and Landgrave, R. (2007). The coasts of our world: Ecological, economic and social importance, *Ecological Economics*, 63(2-3): 254-272.
- Mat Zam, P., Fuad N., Yusoff, A. & Majid, Z. (2018). Evaluating the Performance of Terrestrial Laser Scanning for Landslide Monitoring, *International Archives of the Photogrammetry, Remote Sensing and Spatial Information Sciences*, 42(4/W9).
- Ministry of Oceans and Fisheries (MOF) Coastal Erosion Monitoring Survey in 2017 Ministry of Oceans and Fisheries, (2017).
- Mölg, N. & Bolch, T. (2017). Structure-from-motion using historical

- aerial images to analyse changes in glacier surface elevation, *Remote Sensing*, 9(10): 1021.
- Moon, H.G., Lee, S.M. & Cha, J.G. (2017). Land Cover Classification Using UAV Imagery and Object-Based Image Analysis-Focusing on the Maseo-myeon, Seocheon-gun, Chungcheongnam-do, *Journal of the Korean Association of Geographic Information Studies*, 20(1): 1-14.
- Morton, R.A., Leach, M.P., Paine, J.G. & Cardoza, M.A. (1993). Monitoring beach changes using GPS surveying techniques, *Journal of Coastal Research*: 702-720.
- Muji, A.L. & Tahar, K.N. (2017). Assessment of Digital Elevation Model (DEM) using onboard GPS and ground control points in UAV image processing, 2017 Intelligent Systems Conference (IntelliSys), pp. 835-842.
- Nayak, S., (2002). Use of satellite data in coastal mapping, *Indian Cartographer*, 22: 147-157.
- Nex, F. & Remondino, F. (2014). UAV for 3D mapping applications: a review, *Applied geomatics*, 6(1): 1-15.
- Niethammer, U., James, M., Rothmund, S., Travelletti, J. and Joswig, M. (2012). UAV-based remote sensing of the Super-Sauze landslide: Evaluation and results, *Engineering Geology*, 128: 2-11.
- Papakonstantinou, A., Topouzelis, K. & Pavlogeorgatos, G. (2016). Coastline zones identification and 3D coastal mapping using UAV spatial data, *ISPRS International Journal of Geo-Information*, 5(6): 75.
- Rock, G., Ries, J. & Udelhoven, T. (2011). Sensitivity analysis of UAV-photogrammetry for creating digital elevation models (DEM), *Proceedings of Conference on Unmanned Aerial Vehicle in*

Geomatics.

- Seker, D.Z., Kaya, S., Alkan, R.M., Tanik, A. & Saroglu, E. (2008). 3D coastal erosion analysis of Kilyos-Karaburun region using multi-temporal satellite image data, *Fresenius Environmental Bulletin*, 17(11): 1977-1982.
- Smith, M.W. (2016). 2.1. 5. Direct acquisition of elevation data: Terrestrial Laser Scanning, *Geomorphological Techniques* (Online Edition). London: British Society for Geomorphology. http://www.geomorphology.org.uk/sites/default/files/chapters/2.1.5_TLS.pdf.
- Suarez, S., Cariolet, J. & Fichaut, B. (2010). Monitoring of recent morphological changes of the dune of Vougot beach (Brittany, France) using differential GPS, *Shore and beach*, 78(1): 37-47.
- Thieler, E.R., Himmelstoss, E., A., Zichichi, J.L. & Ergul, A. (2009). The Digital Shoreline Analysis System (DSAS) version 4.0—an ArcGIS extension for calculating shoreline change.
- Topouzelis, K., Papakonstantinou, A. & Doukari, M. (2017). Coastline change detection using Unmanned Aerial Vehicles and image processing technique, *Fresen. Environ. Bull*, 26: 5564-5571.
- Turner, D., Lucieer, A. & Watson, C. (2012). An automated technique for generating georectified mosaics from ultra-high resolution unmanned aerial vehicle (UAV) imagery, based on structure from motion (SfM) point clouds, *Remote sensing*, 4(5): 1392-1410.
- Udin, W.S. & Ahmad, A. (2012). The potential use of rotor wing unmanned aerial vehicle for large scale stream mapping, *Int J Sci Eng Res*, 3: 12.
- Uysal, M., Toprak, A. & Polat, N. (2015). DEM generation with UAV Photogrammetry and accuracy analysis in Sahitler hill,

- Measurement, 73: 539–543.
- Ventura, D., Bonifazi, A., Gravina, M., Belluscio, A. & Ardizzone, G. (2018). Mapping and classification of ecologically sensitive marine habitats using unmanned aerial vehicle (UAV) imagery and object-based image analysis (OBIA), *Remote Sensing*, 10(9): 1331.
- Westoby, M.J., Brasington, J., Glasser, N.F., Hambrey, M.J. & Reynolds, J.M. (2012). ‘Structure-from-Motion’ photogrammetry: A low-cost, effective tool for geoscience applications, *Geomorphology*, 179: 300–314.
- Woodroffe, C.D., (2002). *Coasts: form, process and evolution*, Cambridge University Press.
- Yanagi, H. & Chikatsu, H. (2016). PERFORMANCE EVALUATION OF 3D MODELING SOFTWARE FOR UAV PHOTOGRAMMETRY., *International Archives of the Photogrammetry, Remote Sensing & Spatial Information Sciences*, 41.
- Yang, B.Y. & Hwang, C.S. (2012). Semi-automated extraction of geographic information using KOMPSAT 2: Analyzing image fusion methods and geographic object-based image analysis, *Journal of the Korean Geographical Society*, 47.
- Yoo, C.I. & Oh, T.S. (2016). Beach volume change using UAV photogrammetry Songjung Beach, Korea, *The International Archives of Photogrammetry, Remote Sensing and Spatial Information Sciences*, 41: 1201.
- Yoo, Y.H., Choi, J.W., Choi, S.K., Jung, S.H. (2016). Quality Evaluation of Orthoimage and DSM Based on Fixed-Wing UAV Corresponding to Overlap and GCPs. *Journal of Korean Society for Geospatial Information System* , 24(3), 3–9.
- Zang, Y., Yang, B., Li J. & Guan, H. (2019). An Accurate TLS and

UAV Image Point Clouds Registration Method for Deformation
Detection of Chaotic Hillside Areas, Remote Sensing, 11(6): 647.

